Check for updates

ADVANCED ENGINEERING MATERIALS
www.aem-journal.com

Bessel-Beam Direct Write of the Etch Mask in a Nano-Film of Alumina for High-Efficiency Si Solar Cells

Tomas Katkus, Soon Hock Ng, Haoran Mu, Nguyen Hoai An Le, Dominyka Stonytė, Zahra Khajehsaeidimahabadi, Gediminas Seniutinas, Justas Baltrukonis, Orestas Ulčinas, Mindaugas Mikutis, Vytautas Sabonis, Yoshiaki Nishijima, Michael Rienäcker, Udo Römer, Jan Krügener, Robby Peibst, Sajeev John,* and Saulius Juodkazis**

Large surface area applications such as high efficiency >26% solar cells require surface patterning with 1–10 μm periodic patterns at high fidelity over 1–10 cm^2 areas (before up scaling to 1 m^2) to perform at, or exceed, the Lambertian (ray optics) limit of light trapping. Herein, a pathway is shown to high-resolution sub-1 μm etch mask patterning by ablation using direct femtosecond laser writing performed at room conditions (without the need for a vacuum-based lithography approach). A Bessel beam is used to alleviate the required high surface tracking tolerance for ablation of 0.3–0.8 μm diameter holes in 40 nm alumina Al_2O_3–mask at high writing speed, 7.5 cm s^{-1}; a patterning rate 1 cm^2 per 20 min. Plasma etching protocol was optimized for a zero-mesa formation of photonic-crystal-trapping structures and smooth surfaces at the nanoscale level. The maximum of minority carrier recombination time of 2.9 ms was achieved after the standard wafer passivation etch; resistivity of the wafer was 3.5 Ω cm. Scaling up in area and throughput of the demonstrated approach is outlined.

1. Introduction

Si solar cells are the most developed practical solution for harvesting solar energy and are widely available at a >23% efficiency of solar-to-electrical power conversion at the commercial photovoltaic module level for a household and industrial usage as install-ready 2 m^2 panels.[1–3] The technology of Si solar cells is well matured and produces energy at a cost lower than that traditionally available from national power grids distributing electricity from power stations (coal, gas, nuclear).[4] Recently, the world record performance has been improved from the previously achieved efficiency of Si solar cells 26.81%[5] and stands now at 27.1% measured by the National Renewable Energy Laboratory (NREL).[6] An improvement by

T. Katkus, S. H. Ng, H. Mu, N. H. A. Le, Z. Khajehsaeidimahabadi, G. Seniutinas, S. Juodkazis
Optical Sciences Centre
ARC Training Centre in Surface Engineering for Advanced Materials (SEAM)
Swinburne University of Technology
Hawthorn, Victoria 3122, Australia
E-mail: sjuodkazis@swin.edu.au

D. Stonytė, S. Juodkazis
Laser Research Center
Physics Faculty
Vilnius University
Saulėtekio Ave. 10, 10223 Vilnius, Lithuania

J. Baltrukonis, O. Ulčinas, M. Mikutis, V. Sabonis
Altechna R&D
Mokslininku str. 6A, 08412 Vilnius, Lithuania

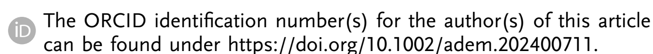
The ORCID identification number(s) for the author(s) of this article can be found under https://doi.org/10.1002/adem.202400711.

© 2024 The Author(s). Advanced Engineering Materials published by Wiley-VCH GmbH. This is an open access article under the terms of the Creative Commons Attribution-NonCommercial License, which permits use, distribution and reproduction in any medium, provided the original work is properly cited and is not used for commercial purposes.

DOI: 10.1002/adem.202400711

Y. Nishijima
Department of Electrical and Computer Engineering
Graduate School of Engineering
Yokohama National University
79-5 Tokiwadai, Hodogaya-ku, Yokohama 240-8501, Japan

M. Rienäcker, U. Römer, R. Peibst
Next Generation Solar Cells
Institut für Solarenergieforschung Hameln (ISFH)
Am Ohrberg 1, 31860 Emmerthal, Germany
E-mail: peibst@isfh.de

J. Krügener, R. Peibst
Institute of Electronic Materials and Devices
Leibniz Universität Hannover
Schneiderberg 32, 30167 Hannover, Germany

S. John
Department of Physics
University of Toronto
60 St. George Street, Toronto, ON M5S 1A7, Canada
E-mail: john@physics.utoronto.ca

S. Juodkazis
WRH Program International Research Frontiers Initiative (IRFI)
Tokyo Institute of Technology
Nagatsuta-cho, Midori-ku, Yokohama, Kanagawa 226-8503, Japan

 © 2024 The Author(s). Advanced Engineering Materials published by Wiley-VCH GmbH

1% in the efficiency took 25 years from M. Green's established 25% benchmark for the monocrystalline Si demonstrated in 1999.[7] None of the modern solar cells perform at the Lambertian (ray optics) limit of light trapping $4n^2$, where n is the refractive index of solar cell material.[8] The practical limit is predicted at 29.1%, which is lower than the theoretical Shockley–Queisser 32% boundary for Si at 1 sun.[7]

Random micro-textured surfaces are used to reduce reflectivity and enhance light trapping; however, they fundamentally cannot perform above the Lambertian limit, which requires harnessing the interference, slow light, and normal-to-parallel redirection of incident light.[9] Such light trapping can be made with photonic crystal (PhC) thin films. It is possible to trap and absorb a much larger number of photons throughout a broad cone of incident angles and a broad range of frequencies, which greatly enhance the overall efficiency of solar cells beyond the Lambertian limit. With 10 μm thickness of Si, it is possible to reach a photocurrent density of 42.5 mA cm^{-2}, close to the 100% solar absorption limit of 43.5 mA cm^2.[9,10] The ability to absorb sunlight well beyond the Lambertian limit, using wave-interference effects, leads to an optimum Si solar cell thickness of only 10 μm instead of previous estimates of about 110 μm using Lambertian light trapping. The bulk Auger recombination, which limits the achievable efficiency of thick Si solar cells, becomes insignificant for thin Si when 98% of available sunlight is absorbed within only 10 μm of Si.[9]

Harnessing of wave properties provides an enhanced absorbance at strongly localized resonances, especially at the energies close to the bandgap.[11] The first experimental demonstration of light absorption above the Lambertian limit in a Si slab was made using PhC structures with etch masks patterned by electron beam lithography with subsequent wet etching in KOH and plasma.[12] The possibility to define etch mask by stepper projection lithography and direct laser write (DLW), which both have the capability of larger area patterning, was demonstrated for a Si wafer.[13] The same PhC pattern, which performed the above Lambertian light trapping, was made on actual Si solar cells and compared to a neighboring central cell of the same geometry and structure on the same wafer but without PhC patterns (7 solar cells in total per wafer).[14] This first demonstration of PhC light trapping on a Si solar cell showed 23.1% efficiency on the PhC textured region (independently verified by ISFH CalTeC) as compared to 21.1% for the neighboring central cell on the same wafer. Another active trend in solar cells is making them thin, flexible, and low weight[15] including use of 2D materials.[16] PhC light trapping can be used to achieve 95% absorption of light within 10 μm thick Si solar cell to expand their application potential.[17] Flexible Si solar cells of 54 μm thickness showed the highest power-to-weight ratio of 1.9 W g^{-1} for 274 cm^2 area;[18] the light-to-electrical power conversion was 26.06%.

Both, wet and dry etching of Si strongly affects surface quality, which is evaluated by the minority carriers' lifetime τ_m. Also, Ohmic contacts are of paramount importance to reduce losses due to Joule heating. Even a KOH etch for a few minutes reduces τ_m from 10 to 7 μs at low p-doped Si.[19] Fs-laser-ablated Si showed a reduction of τ_m up to a factor of two after plasma etch for the maskless case of pattern definition by femtosecond-laser ablation.[20] When Cr–mask was used, the τ_m was reduced up to 2 μs from 12 μs on the untreated Si surface.[20] For high-efficiency Si solar cells, $\tau_m \geq 2$ ms is required,[14] which is by one order of magnitude higher than those observed on as-etched surfaces. The τ_m defines the surface recombination velocity SRV $\propto 1/\tau_m$, which has to be ≤ 1 cm s^{-1} and this condition is more demanding for thin solar cells;[21] SRV up to 100 cm s^{-1} sill cause no significant reduction of efficiency as was found by simulations.[21,22] Low SRV 1 cm s^{-1} rate is achievable by low temperature 175–200 °C hydrogenation[23] of high performing 26% (Panasonic 2013) Si/a-Si:H heterojunction solar cells.

Here we demonstrate the fabrication of PhC pattern for light trapping on the face surface of actual Si solar cells. A dielectric Al_2O_3 mask of tens of nm thickness was laser ablated by ultrashort laser pulses (515 nm/167 fs) using an axicon lens for the formation of the Bessel beam.[24] Ablated holes in the mask had a diameter smaller than the diffraction limit at the focusing conditions due to the threshold effect, i.e., the ablation threshold of the mask was exceeded only in the optimal center of the focal spot. The dry plasma etching protocol was optimized for a nano-smooth surface of PhC pattern with minimal ridges between inverted pyramidal pits of PhC, without apparent debris and oxidized nanoscale regions. Optimization of plasma etching over a wide parameter space of chemistry used, process pressure, and flow rates of gasses is presented. The PhC light-trapping structures were fabricated on polysilicon on oxide-interdigitated back-contacted–$POLO^2$–IBC cell; such cells have the potential to perform at >26% efficiency of solar-to-electrical power conversion.[25]

2. Experimental Section

The thickness of the electron (e)-beam (JKLesker AXXIS)-coated Al_2O_3 was determined by ellipsometry (Woolam, VASE). Masks of 30 and 40 nm were investigated for optimization of the laser ablation and plasma etch protocols. The refractive index $n + i\kappa \approx 1.595 + i0.011$ of Al_2O_3 was determined by ellipsometry. Thinner 20 nm masks showed up to a few percent reduction in κ while n was proportionally larger.

Si wafers (catalog number 783, University Wafer Inc.) were p type (Boron doped) with resistivity $1 - 10\,\Omega$ cm and were close to that of the actual $POLO^2$–IBC p-type solar cells. The wafer's primary flat (see inset in **Figure 1**) was used to align the PhC mask pattern. The alignment is critical for plasma etching while low ICP power is used and the etching result resembles structures, similar to those obtained by wet etching in KOH with a distinct pattern of inverted pyramids. Imperfect mask alignment causes defects in mesa ridges and corner posts, which should be minimized for the best-performing light trapping.

The axicon used in this study was designed for $\lambda = 515$ nm wavelength and it was femtosecond-laser inscribed inside the bulk of silica glass. The form birefringence of nano-gratings was used to engineer the refractive index of concentric grating for the required phase retardance. The cone angle of the flat axicon corresponded to 178°. A $f = 400$ mm lens combined with ×20 magnification; $NA = 0.4$ objective lens was used to scale down the Bessel beam using an optical 4 F relay scheme.

© 2024 The Author(s). Advanced Engineering Materials published by Wiley-VCH GmbH

15272648, 2024, 21, Downloaded from https://onlinelibrary.wiley.com/doi/10.1002/adem.202400711 by Vilnius University, Wiley Online Library on [13/11/2024]. See the Terms and Conditions (https://onlinelibrary.wiley.com/terms-and-conditions) on Wiley Online Library for rules of use; OA articles are governed by the applicable Creative Commons License

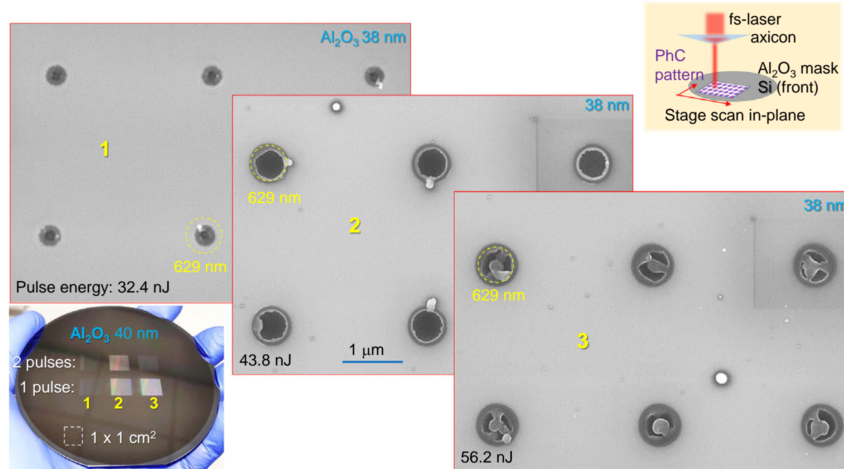

Figure 1. 1–3) SEM images of 38 nm thick Al_2O_3 film ($n + i\kappa = 1.595 + i \times 0.01054$) ablated using single pulses of 515 nm/167 fs laser (Pharos PH-10 W-SP, Light Conversion) light shaped into Bessel beam using axicon optics. Pulse energies were $E_p = 32.4, 43.8, 56.2$ nJ—as marked on each SEM image. The 629 nm diameter circle markers correspond to the observed laser modified spot size at the smallest pulse energy. This diameter is smaller than the $1/e^2$–intensity cross section of the central core of the Bessel beam which was 880 nm; top right inset—schematic representation of Bessel beam formation by axicon used for mask patterning; bottom left inset—photo of the alumina-coated silicon wafer with 1×1 cm^2 areas laser patterned using one and two pulse per site modes and pulse energies listed earlier.

The first minimum of the Bessel intensity profile is at $d^B_{min} = 0.383\lambda/\sin\gamma$, where $\lambda = 515$ nm is the laser wavelength, $\gamma = 18.46°$ is the cone angle with respect to the optical axis along beam propagation; $d^B_{min} = \frac{4.816}{k_\perp}$, where $k_\perp = k\sin\gamma$ is the wavevector component perpendicular to the propagation ($k = 2\pi/\lambda$). The final cone angle on the sample was $\gamma = 18.46°$, the diameter of $d^B_{min} = 1.24$ μm at the first minimum or 0.88 μm at $1/e^2$–intensity level. The length of the non-diffracting Bessel beam zone was ≈400 μm.

The central spot as well as every ring of the Bessel beam in the focal region carry the same amount of energy. The average intensity and fluence per pulse of the optical $E_p = 44$ nJ energy used in mask patterning are estimated considering the central spot of the diameter equal to the first minimum d^B_{min}: $I_p \equiv F_p/t_p = 21.76$ TW cm^{-2} and $F_p = E_p/(\pi[d^B_{min}/2]^2) = 3.63$ J cm^{-2}, respectively, for the $t_p = 167$ fs pulse ($ct_p = 50$ μm axial extent). This calculation is carried out the same way as for the Gaussian pulse and can be used for protocol development. For the actual comparison of fluences between Bessel and Gaussian pulses, the axial extent of the beams can be compared since all the depth of focus (DoF) of a Bessel beam carries laterally distributed rings that converge onto the optical axis. The same focal spot for a Gaussian beam can be achieved with focusing using NA_G lens defined by $d^B_{min} = 1.22\lambda/NA_G$. Then, the DoF or double the Rayleigh length $2z_R = 2\pi[d^B_{min}]^2/\lambda = 18.8$ μm. This is 21 times shorter than the DoF of the Bessel beam. Hence, the corresponding fluence of the Bessel beam reduced by this factor is 0.17 J cm^{-2} and is close to the ablation threshold of Si. For the Gaussian pulse, the ablation threshold of Si is 0.2 J cm^{-2}.[26] Laser patterning of the alumina mask was carried out using single pulses of $\lambda = 515$ nm wavelength and $\tau = 167$ fs pulse duration (Pharos PH-10 W-SP, Light Conversion). The sample was placed on a porous stone sample holder and secured using vacuum suction. Patterning was performed using linear nanopositioning stages (ANT130XY, Aerotech) moving in the *xy* plane. Focusing objective, mounted on *Z*-axis stage (ANT130LZS, Aerotech), was kept stationary. The stage controller (XR3, Aerotech) equipped with position synchronized output (PSO)-feature-synchronized laser triggering to the motion of nanopositioning stages. Fabrication sequence was defined and controlled from SCA software (WoP, Ltd.).

Sinton WCT-100 was used to determine the minority carrier lifetime τ_m via inductive detection of the cumulative recombination currents in the bulk and on the surface of solar cell or Si wafer. A light flash creates electron–hole pairs (e–h) with concentration $\Delta n = \Delta p$, which are much smaller than those due to doping (n or p). A short minority carrier lifetime τ_m is related to the high surface recombination velocity SRV and limits collection of photo-carriers, i.e., reduces the efficiency of light-to-electricity power conversion.

3. Results

For this study, we chose an Al_2O_3 mask due to its mechanical strength even at nano-film conditions and being compatible with antireflection coating of Si solar cells. Metal masks such as Cr or Ti make good adhesion to Si and can withstand plasma etch used in this study;[13] however, they can deteriorate the performance of Si in terms of increased surface recombination velocity. Also, a hard mask of 20 nm thick silicon nitride was used to ablate 600 nm diameter holes by femtosecond laser for subsequent anisotropic wet etch of Si in KOH;[27] Gaussian laser pulses were utilized. Similar patterns can be made by high-resolution lithography;[28] however, here, we focus on patterning without the conventional lithography approach which is not amenable to large-area solar cells.

© 2024 The Author(s). Advanced Engineering Materials published by Wiley-VCH GmbH

15272648, 2024, 21, Downloaded from https://onlinelibrary.wiley.com/doi/10.1002/adem.202400711 by Vilnius University, Wiley Online Library on [13/11/2024]. See the Terms and Conditions (https://onlinelibrary.wiley.com/terms-and-conditions) on Wiley Online Library for rules of use; OA articles are governed by the applicable Creative Commons License

15272648, 2024, 21, Downloaded from https://onlinelibrary.wiley.com/doi/10.1002/adem.202400711 by Vilnius University, Wiley Online Library on [13/11/2024]. See the Terms and Conditions (https://onlinelibrary.wiley.com/terms-and-conditions) on Wiley Online Library for rules of use; OA articles are governed by the applicable Creative Commons License

3.1. Bessel Beam Patterning of Al_2O_3 Mask

The DLW by 515 nm/167 fs laser pulses with Bessel beam focusing was carried out on blank Si wafers coated by 30 ± 2 and 40 ± 2 nm Al_2O_3 films deposited by electron (e)-beam evaporation. Single and double pulse per ablation site was used to write $1 \times 1\,cm^2$ masks at $7.5\,cm\,s^{-1}$ scan speed; the laser repetition rate was 0.6 MHz. It takes 20 min to pattern a $1 \times 1\,cm^2$ area. These scan and repetition rate conditions were chosen for the reliable positioning of ablation sites within ± 20 nm tolerance from the designated positions (laser trigger on position in the PSO mode of writing) on a square grid with $\Lambda = 3.1\,\mu m$ period as required for the PhC light trapping. The writing speed can be further increased since 30 nm positioning errors were observed for the maximum tested writing speed of $10\,cm\,s^{-1}$; further increase of a writing speed will be studied separately. The positioning errors translate into mesa errors, especially at the corners of the etched pit. The orientation of the mask was aligned to the base cut of Si wafer to have the best etching conditions and smallest mesa regions. Irradiation of two pulses per ablation site caused a larger debris field as well as holes in the mask clogged by droplets of quenched melt (similar as in region 3 of Figure 1). Notably, debris on a mask and small changes in the shape of the hole in mask were still acceptable for plasma etch. Thinner 30 nm Al_2O_3 masks showed less debris and smaller holes; however, this thickness value was not selected for the final fabrication on Si solar cells due to being prone to fracture when undercut etched. Thicker 50 nm masks showed the presence of brittle fracture at the rim of the opening and larger debris fields.

3.2. Plasma Etch: Optimization of Conditions

First, different chemical mixtures for dry plasma etching were investigated with the aim of identifying those that yield the smoothest surfaces of Si production. One of the simplest mixtures of SF_6/O_2 was the most promising since the addition of CF_4 and/or CHF_3 resulted in more nano-rough surfaces even if the etch rate was faster (for illustration see selected conditions shown in Figure A1).

The parameter space of optimal etch protocol was investigated with a change of inductively coupled plasma (ICP) power, which favors isotropic all-direction material removal as well as bias power, which defines anisotropic directional (between electrodes) etching; see Figure A3a for the surface produced by the optimized etch protocol. **Figure 2** shows optical images of pattern evolution at large ICP power with bias at 0 W. When the corner posts of Si below the mask become sub- 1 μm in the lateral cross section, they appear colorful under optical inspection with an objective with numerical aperture NA = 0.9 (see inset in Figure 2d). Different colors are related to the small differences in shape of pillars which evolves from small changes of ablated holes in the mask (see scanning electron microscopy [SEM] inset

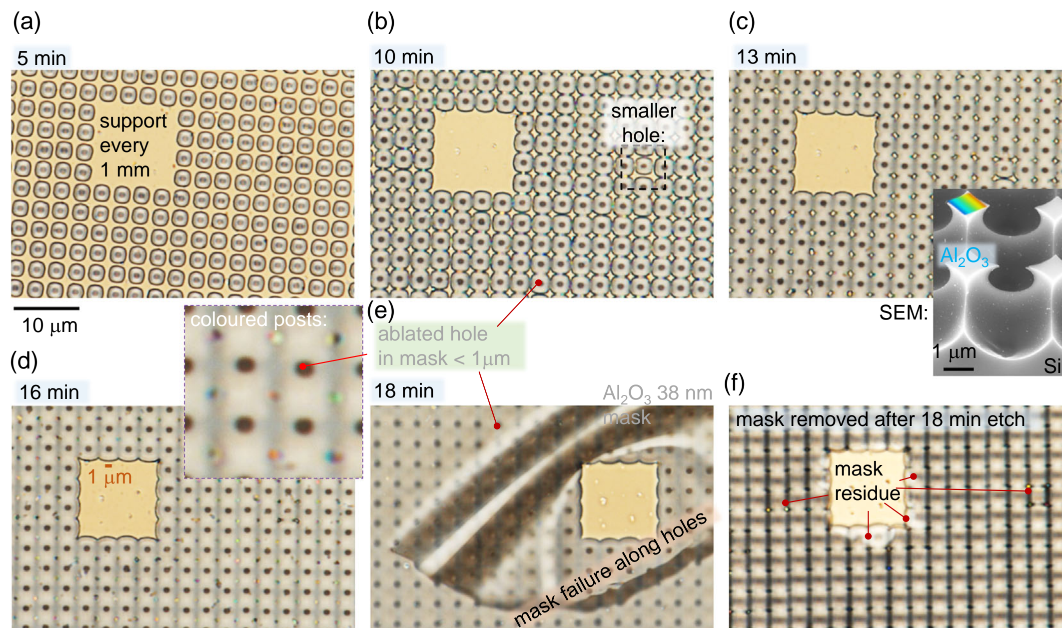

Figure 2. a–f) Optical microscope images of photonic crystal (PhC) light-trapping surface dry-etching evolution in time. Images were taken using Nikon LV100POL microscope with an objective lens of numerical aperture NA = 0.9. Labels indicate cumulative etching time up to 18 min. The optimized protocol of the isotropic reactive ion etching (RIE-101iPH, Samco) at high etch rate was carried out at 200 W of inductively coupled plasma (ICP) power and at 0 W Bias power. Gas flows used were 50/5 sccm of, respectively, SF_6/O_2 at the process pressure of 2 Pa with He lower electrode cooling enabled. The inset in (c) is a scanning electron microscopy (SEM) image of a PhC etched in SF_6 plasma for 15 min. It illustrates the mesa structures and Al_2O_3 mask adhered on corner pillars surrounding the square pits. The rainbow marker highlights locations that appeared colored under the optical microscope. When those corner structures become smaller than 0.5 μm in size (close to the diffraction limit of optical observation $0.61\lambda\,NA^{-1}$ at central visible wavelength $\lambda = 530$ nm—green), they appear colorful (see inset in (d)). This condition may be used as a reference for etching process termination timing. Over etching causes mask release and likely failure as shown in (e). The 38 nm alumina mask was removed by ultrasonic agitation in isopropanol. Mask writing was done using Bessel beam.

© 2024 The Author(s). Advanced Engineering Materials published by Wiley-VCH GmbH

15272648, 2024, 21, Downloaded from https://onlinelibrary.wiley.com/doi/10.1002/adem.202400711 by Vilnius University, Wiley Online Library on [13/11/2024]. See the Terms and Conditions (https://onlinelibrary.wiley.com/terms-and-conditions) on Wiley Online Library for rules of use; OA articles are governed by the applicable Creative Commons License

image in (c)). This stage of color appearance in pattern formation is indicative that the plasma etch should be finished, since the Al_2O_3 mask breaks when the undercut etch progresses and some of the posts will not support the mask (38 nm thick in Figure 2). A mask is removed by immersion of the sample into an ultrasonic bath of isopropyl alcohol (IPA) for 5 min. If the mask is not fully removed from the Si post, it appears colorful under optical inspection. Since alumina is part of the antireflection coating in the final design of the solar-trapping surface, this is not considered a critical issue. For the final etch protocol, the slow etch rate was used. This resulted in posts of the same color (dark blue) under microscope observation, which indicates size and shape uniformity (Figure A6).

The PhC pattern was defined by etch mask on a $1 \times 1\,cm^2$ area which had unablated 4×4 holes every 1 mm in x and y directions of the pattern by design. Those posts were added to support the Al_2O_3 membrane during dry plasma etch (this action is illustrated in Figure 2e where mask is fixed to the post after it fails in the free-suspended region). Their contribution to an increased reflection from Si solar cell with PhC light-trapping patterns can be considered small.

Even though ICP is known for favoring isotropic etch, at lower ICP powers, the etch becomes slower and the crystalline structure of Si becomes prominent on the etched surface (Figure A2). We chose low 30 W ICP power for the optimized protocol and no oxygen was used to reduce surface oxidation, which caused nonhomogeneous islands/residue formation apparent under SEM inspection.

Next, the influence of the bias power was investigated. **Figure 3**a–c shows side-view cross sections aligned to the original surface of Si etched under increasing bias, i.e., directional plasma bombardment of the surface. Elliptical markers are added as eye guides to facilitate a small increase of depth at large powers. The effect of bias was not very prominent understandably due to the small sub-1 μm opening in the mask through which the etching of Si was made. An increased bias power also affected the thickness of Al_2O_3 mask, which is undesirable. Zero bias was used for the final protocol. During SEM observation of samples after different times of plasma etch, it was observed that charging nano-debris are increasingly present (Figure 3c,d) after repeated exposures of the sample to the air (in class 1000 cleanroom). This residue of etchants or/and oxidized Si is minimized with reduced steps of air exposures as in the final fabrication. With a lower content of oxygen in SF_6/O_2 mixture, the surface had less of the oxidized residue and smoother surfaces. For the final protocol, no oxygen was selected.

The process pressure in the chamber is another important parameter, especially due to the ICP-dominated etch, which was selected for the PhC pattern. The He gas flow below the sample was used for cooling the sample and was negligibly contributing to the process pressure. The reactivity of plasma and the isotropic nature of etching depended on the process pressure (Figure A3). The low pressure facilitated the smooth morphology of Si with the largest depth (Figure A3), which are both desirable virtues selected for the final protocol (shown in Figure A3a). The sensitivity of etched surface roughness and presence of oxidized textures is illustrated in Figure A4 where ambient pressure changes are shown to strongly affect the morphology at larger ICP powers and O_2 flow even at 0 W bias.

The key attribute of the proposed plasma etch protocol using a large area laser patterning of 40 nm thick Al_2O_3 mask is timing. Etching should be stopped at the moment of the smallest pillar posts' formation (**Figure 4**). The posts provide mechanical support for the mask. Undercut etching and narrow mesa formation are already present even before posts are etched out. With the posts of 150 ± 50 nm in cross section, the deepest PhC pattern is formed with minimized mesa ridges. The final optimized recipe of PhC etch was selected for the slow etch, which caused the formation of the smallest posts (same deep blue color; Figure A6), no oxygen in the etching gas mixture (only SF_6), 0 W bias, 30 W ICP, and 1 Pa of process pressure. Such etching revealed the (111) Si planes typically observed in wet KOH etching. Minimum oxidation debris is formed on the surface, which is subsequently processed via wet etch KOH passivation and antireflection coating steps for the final solar cell.

Figure 5a shows the appearance of etched PhC pattern using Al_2O_3 mask patterned by femtosecond-Bessel beam on the surface of actual solar cells. The total etch time to achieve minimal mesa ridges (Figure 5b) was approximately twice as long for the entire Si wafer as compared with the test samples of

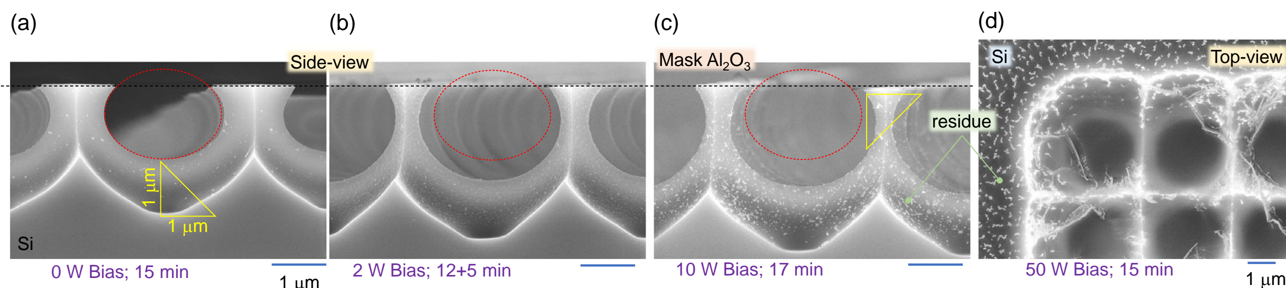

Figure 3. SEM images of etch cross sections at different Bias powers: a) 0 W, b) 2 W, c) 10 W, and d) 50 W (top view in (d)). Etch time is shown at the bottom of panels; when repeated etching was applied, times were shown with a summation marker "+" in (b). RIE was carried out at 2 Pa process pressure, 200 W ICP power at 50/0 sccm SF_6/O_2 gas mixture. For comparison of evolution of etched pattern oval and right-triangular markers of the same size are shown in (a–c). Thickness of Al_2O_3 mask was 28.4 nm; mask writing was with Bessel beam. The amount of dry-etching residues correlates with bias power level, most probably. Note that the residues which appear as white particulates in SEM images are caused by exposure of etched surface to room conditions and was becoming increasingly apparent under repeated sample's inspections. Formation of residue can be avoided when all the etch process is carried out in a single step.

 © 2024 The Author(s). Advanced Engineering Materials published by Wiley-VCH GmbH

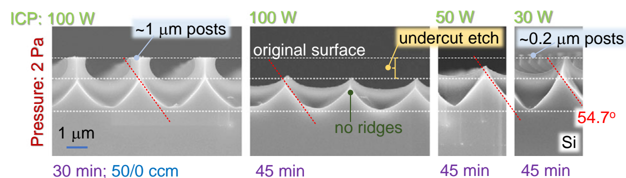

Figure 4. Evolution of under etching at decreasing ICP power from 100 to 30 W (the final optimized condition) at 0 W bias; SF_6/O_2 50/0 sccm, pressure of 2 Pa. The under etching removes the post regions. The minimum size of the posts also corresponded at the largest depth of the etched pattern (appeared colorful under optical observation; Figure A6). The timing of etching is the main parameter for the optimal conditions of PhC formation. Thickness of Al_2O_3 mask was 38 nm; mask writing was with Bessel beam. The angle of 54.1° between top surface (100) plane and (111) plane is shown by dashed-inclined lines.

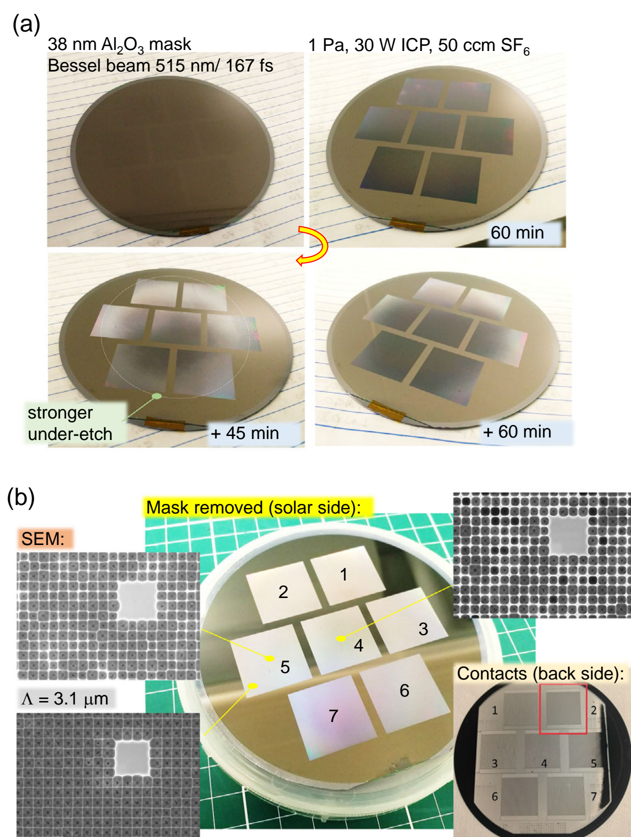

Figure 5. PhC light trapping for polysilicon on oxide-interdigitated back-contacted–POLO²–IBC cell. The thickness of a Si solar cell is 190 μm. a) The mask (38 nm thick Al_2O_3) was patterned by femtosecond-laser direct write with Bessel beam 515 nm/167 fs, pulse energy $E_p = 43.8$ nJ over 2.2×2.2 cm² areas on the front side above of an integrated Si cells with backside contacts. Plasma etches and PhC pattern evolution were observed at different paused times during etching. The optimized protocol was used: 1 Pa process pressure, 30 W ICP power, SF_6/O_2 50/0 ccm flow rate. b) The center image is the final PhC-trapping surface after mask removal in an IPA ultrasonic bath. Insets show SEM images of the final PhC light-trapping surface at different locations. There was a slight difference in terms of the under-etch conditions across the wafer recognizable in a) optical and b) SEM images. The right-bottom inset image shows the backside contacts.

$\approx 1 \times 1$ cm² patterned masks used for the development of the etch protocol; mesa ridges contribute to unwanted reflection from the front surface. However, the quality of the etched surface, mechanical integrity of the mask, and residue formation were the same as per the optimized recipe. One important difference of the wafer scale etch was the slight radial variation of undercut etching, which is an important and favorable attribute of the plasma processing of PhC light-trapping surface (Figure 5). Dedicated wafer-size optimization of the etch protocol is required. For that, we foresee the requirement of a mechanically stronger mask for longer etching with an undercut etch conditions as discussed in the next section.

3.3. Minority Carrier Lifetime

In the best performing POLO²–IBC solar cell with PhC light trapping $\eta = 23.1\%$,[14] $\tau_m \approx 2.3$ ms was achieved over 2×2 cm² area after a prolonged 300 min isotropic etch in the ammonia peroxide mixture (APM) with an etch rate of 1 nm min^{-1}; the short current density $J_{sc} = 40.2$ mA cm^{-2}. The initial values $\tau_m = 0.35$ ms for plasma-treated surface and J_{sc} become 40.83 mA cm^{-2} after the first (from four) 75 min step of APM passivation etch. Noteworthy, APM wet etch caused a slight increase in overall reflectivity from 11.2% to 13.1%, where the reflection and charge carrier lifetime were determined with AlOx passivation at each step.

Figure 6 shows the minority carrier lifetime τ_m dependence on the density of photoexcited carriers Δn (Figure 6a) and spatially resolved maps (Figure 6b) for Bessel beam patterned cells. The same APM passivation etch was carried out as for the cells previously patterned with Gaussian beam and plasma etched.[14] The maximum of $\tau_m \approx 2.9$ ms lifetime was achieved. This is comparable with the high efficiency 26.1% cell where 2.1 ms time was obtained for random micro-pyramidal surface texture; note that the resistivity of the wafer was 1.5 Ω cm[25] while 3.5 Ω cm in this study.

4. Discussion

4.1. Bessel Beam Patterning on Front Side of POLO²–IBC Cell

Figure 5 and A7 show the currently achieved patterning of polysilicon on oxide-interdigitated back-contacted– POLO²–IBC cell. This POLO²–IBC architecture, same materials, and fabrication protocols achieved 26.1% solar-to-electric power conversion efficiency.[25] The mask writing throughput by the Bessel beam was 1 cm² in 20 min. A further increase is possible by combining *xy*-stage scan with Galvano-mirror scanning,[29] especially, due to the stitch-less mode of writing over large areas. The actual increase in throughput of 2D patterning depends on the pattern complexity; however, it is expected to be a considerable factor based on the 3D polymerization study.[29] For the Bessel beam with the axial extent of the 400 μm used in this study, there is a high tolerance for axial position of the focal region on the Si surface with 40 nm thick mask even for an existing tilt of the sample and surface unevenness. Curved surfaces can be, in principle, patterned with the Bessel beam. The virtue of large DoF of Bessel beam is particularly valuable for large area patterning and

 © 2024 The Author(s). Advanced Engineering Materials published by Wiley-VCH GmbH

15272648, 2024, 21, Downloaded from https://onlinelibrary.wiley.com/doi/10.1002/adem.202400711 by Vilnius University, Wiley Online Library on [13/11/2024]. See the Terms and Conditions (https://onlinelibrary.wiley.com/terms-and-conditions) on Wiley Online Library for rules of use; OA articles are governed by the applicable Creative Commons License

15272648, 2024, 21, Downloaded from https://onlinelibrary.wiley.com/doi/10.1002/adem.202400711 by Vilnius University, Wiley Online Library on [13/11/2024]. See the Terms and Conditions (https://onlinelibrary.wiley.com/terms-and-conditions) on Wiley Online Library for rules of use; OA articles are governed by the applicable Creative Commons License

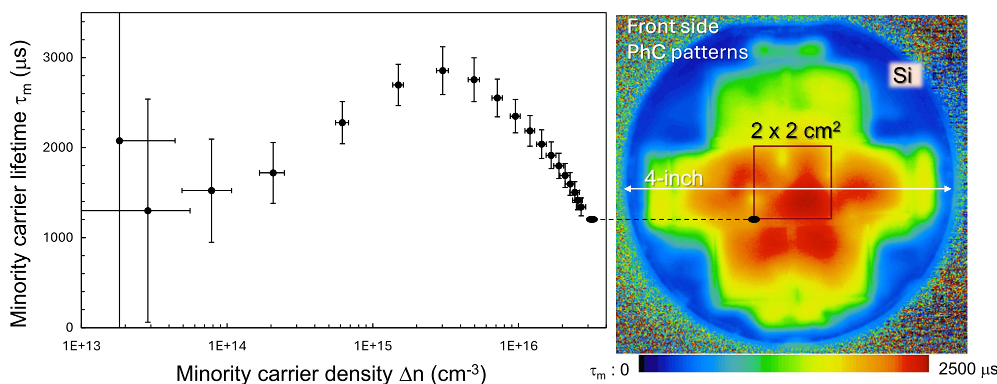

Figure 6. a) The photoinduced carrier density dependence in the selected central cell (region 4 in Figure 5) on the 190 μm thick wafer with the POLO–IBC Si solar cells (see $2 \times 2\,cm^2$ marker on the wafer map in (b)). b) Minority carrier spatially resolved lifetime maps under 0.72 sun illumination. PhC light-trapping regions were patterned with femtosecond-laser Bessel beam by ablation of alumina mask and plasma etched for the minimal mesa widths. The resistivity of wafer was 3.5 Ω cm.

large speed mask writing when vertical displacements of the surface of solar cell are present and/or changing during laser writing. In this study, the pulse duration corresponds to 50 μm in air as it travels through the non-diffracting section of 400 μm.

What was observed in the full wafer etch (Figure 5) is a twice longer etch time required for the same depth of the PhC pattern. This longer etch puts more stringent requirements against mechanical failure of the patterned mask. A higher ICP power would facilitate a faster etch rate, however, mask thinning with more erosive plasma would take place.[20]

4.2. Mask with Distributed Support: Numerical Modeling of Light Trapping

A practical solution to make better support for the etch mask would be to omit every second ablated hole in every second line (see concept in **Figure 7**a). Finite difference time domain (FDTD) modeling (Lumerical, Ansys) of a toy model of such PhC texture for 3 μm thick Si is shown in Figure 7b for the spectra of absorption and scattering cross sections. Such a pattern has very similar cross sections as compared with an inverted pyramid PhC. **Figure 8** shows light intensity distributions at very different wavelengths for a normally incident plane wave. The incident intensity is normalized and the $|E|$ shows the enhancement of electrical E-field due to interference inside Si especially at the longer wavelengths. This toy-model simulation qualitatively captures the wave nature of PhC light trapping which can perform above the Lambertian $4n^2$ ray optics trapping used in solar cells.[12]

Maskless patterning of Si surface using ablation by interference of three[19] or more[30] laser beams was proposed for the definition of etching sites on Si for inverted pyramidal structures produced by wet etch. Different wet etch solutions can be used for anisotropic etch of Si.[31] Plasma etch can also form a pattern of inverted pyramids after the femtosecond-laser direct write defines it by ablation.[20] Laser-marked ablation sites have nano-volumes of structural defects[19] (nanosecond-laser ablation) and nano-cracks[31] (femtosecond-laser ablation), which

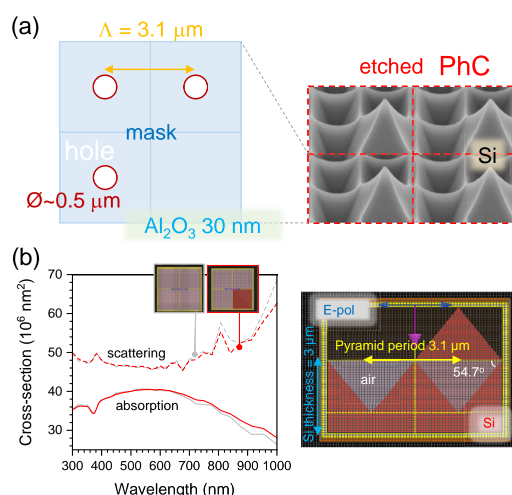

Figure 7. a) Concept for a better mechanical support of the nano-film mask over large areas for a deeper etch of PhC patterns: laser inscribed mask in 30 nm thick Al_2O_3 with periodic micro-posts (not ablated sites). b) Finite difference time domain (FDTD) calculations of absorption and scattering cross sections for the pattern in (a) and same geometry only with four pyramidal pits. Periodic boundary conditions are applied for the *xy* plane (lateral dimension) and perfectly matching layers in the longitudinal direction (along light propagation). The thickness of the cell is 3 μm; Si permittivity $(n + i\kappa)^2$ is from the Lumerical, Ansys database. Geometrical cross section (footprint) of the pyramid (or inverted pyramid) is $9.61 \times 10^6\,nm^2$.

can be located up to few-hundreds nanometers below surface in the case of maskless laser patterning. Those defect rich nano-volumes are etched out in KOH. Similarly, for plasma etch when transparent alumina mask is used as in this study, the laser affected regions are removed during the formation of inverted pyramids.

The proposed model of the etch mask is amenable over large areas (10 in wafer) and larger. Due to a mechanically stronger mask, it can potentially be thinner and smaller ablation holes can be printed if required for a smaller PCh period. The very same etch chemistry at a higher ICP and bias were also tested

 © 2024 The Author(s). Advanced Engineering Materials published by Wiley-VCH GmbH

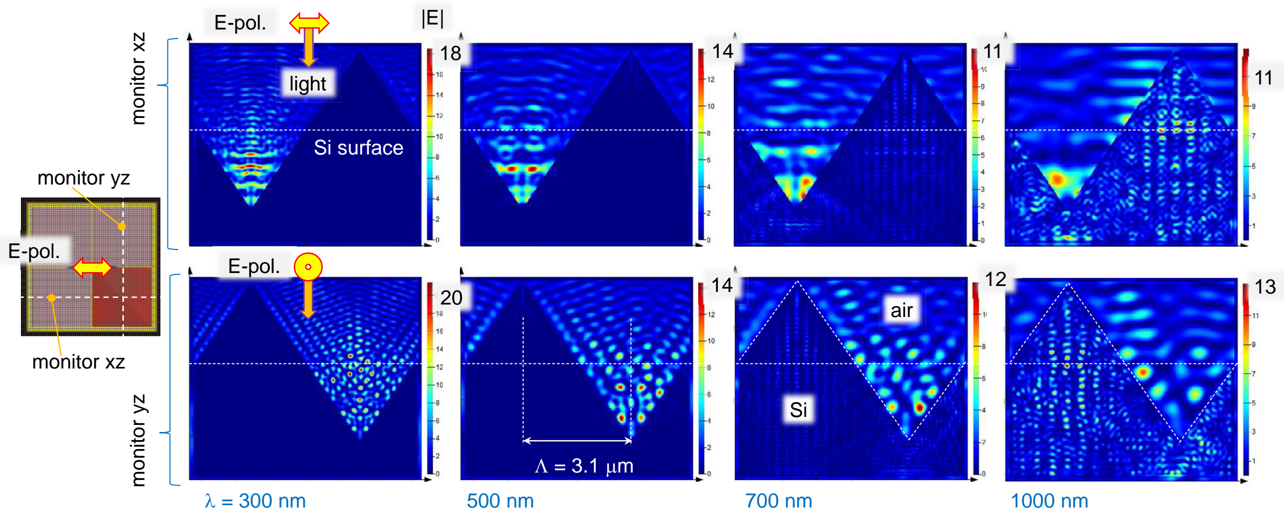

Figure 8. Light intensity enhancement at two cross sections (monitors) at difference wavelengths simulated by FDTD with periodic boundary conditions applied for the lateral dimension and perfectly matching layers in the longitudinal direction (along light propagation); same geometry as in Figure 7. The thickness of the cell is 3 μm; Si permittivity $(n + i\kappa)^2$ is from the Lumerical, Ansys database. Incident light intensity $|E|^2 = 1$.

for thinning of Si from 0.5 to 0.1 mm (Figure A8). Such thinning opens the possibility to use a compatible process to thin Si solar cells with backside contacts to the required thickness before adding the PhC-trapping surface, which is the most efficient in thin tens-of-micrometers Si solar cells.[17]

4.3. Surface Defects Due to Plasma Etch

Plasma etch is known to cause surface defects due to ion bombardment and implantation of contaminants with penetration from nanometers to a micrometer.[32,33] The surface defects usually removed via a defect-removal etch (KOH, HNO_3 :HF, etc.).[34,35] Hence, we used here the zero-bias plasma etch to reduce directional bombardment of surface by ions and APM defect-removal wet etch. ≈300 nm isotropic APM etch resulted in defect-free performance of front surface of solar cell;[14] details on determination of efficiency and electrical characteristic of 23.1% $POLO^2$–IBC cell will be reported elsewhere. The open-circuit voltage V_{oc} was reduced for nanosecond-laser written mask and KOH etch.[19] In the case of $POLO^2$–IBC best performing cell with a random pyramidal texture (without PhC light trapping), $V_{oc} = 730.2$ mV and $J_{sc} = 42.2$ mA cm^{-2} (the fill factor FF = 84.44% and efficiency 26.02%). For the best performing cell with PhC light trapping, $V_{oc} = 710$ mV and $J_{sc} = 39.9$ mA cm^{-2} (the fill factor FF = 81.5% and efficiency 23.1%) while a neighboring wafer-central cell with a flat non-textured surface $V_{oc} = 720.5$ mV and $J_{sc} = 36.21$ mA cm^{-2} (FF = 81% and efficiency 21.1%).[14]

5. Conclusions and Outlook

Direct laser writing of a hard etch mask using ultrashort femtosecond-laser pulses is demonstrated for fabrication of PhC light-trapping surface on actual high-efficiency polysilicon on oxide-interdigitated back-contacted– $POLO^2$–IBC cells. Using tens-of-nanometers Al_2O_3 hard mask ablated by femtosecond-laser Bessel beam at high 7.5 cm s^{-1} scan speed at room conditions makes this approach scalable for solar cell applications. Periodic PhC patterns are required to break the ray optics Lambertian limit of light trapping. A detailed account of explored parameter space to optimize plasma etching is presented for different etch chemistries, powers of ICP and bias, and process pressure. Only an optical inspection of the evolution of PhC formation is required to determine the required etching time and degree of under etching.

Scalability of such lithography-less and vacuum-less micro-patterning of PhC textures over even larger areas is outlined and the feasibility of light trapping based on wave nature of light is qualitatively evaluated using a numerical toy model. Detailed performance of these PhC – $POLO^2$–IBC cells will be reported in a dedicated study. Here, the experimental account for the selection of hard-mask thickness for direct laser writing by Bessel beam and dry plasma etching were all synergistically optimized and solved for an upscalable application. The optimized dry-etch recipe uses ICP plasma without bias power resulting in minimal plasma damage to the etched surface.

Appendix

Here, a set of supplementary figures illustrates and summarizes experimental observations with a selection of qualitative illustrations of the main consequence of particular etch parameter change. Figure captions are self-explanatory with technical details and main conclusions.

© 2024 The Author(s). Advanced Engineering Materials published by Wiley-VCH GmbH

15272648, 2024, 21, Downloaded from https://onlinelibrary.wiley.com/doi/10.1002/adem.202400711 by Vilnius University, Wiley Online Library on [13/11/2024]. See the Terms and Conditions (https://onlinelibrary.wiley.com/terms-and-conditions) on Wiley Online Library for rules of use; OA articles are governed by the applicable Creative Commons License

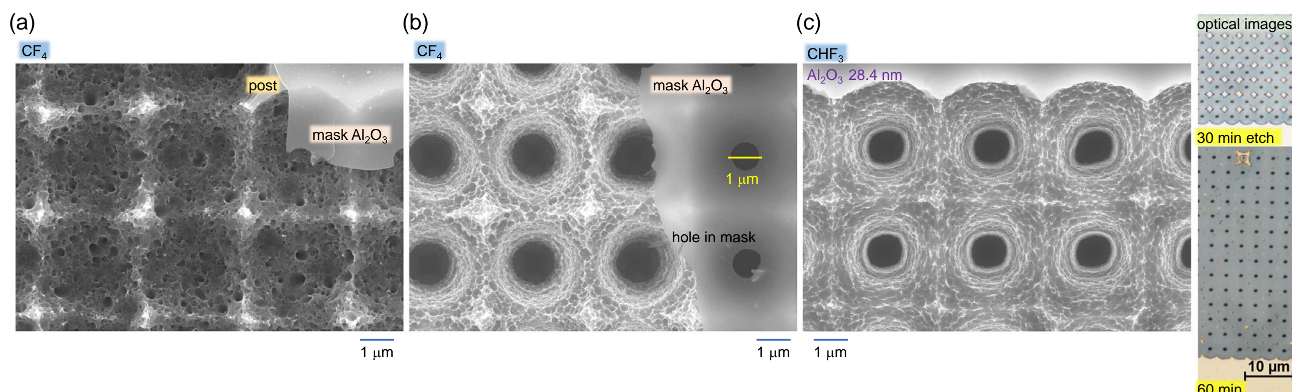

Figure A1. Typical PhC structures at different etch chemistries. a) CF_4 test: 2 Pa process pressure, 200 W ICP, 0 W Bias, 50/5 ccm of CF_4/O_2 for 60 min. Strong under etch. Thickness of Al_2O_3 mask 37.6 nm, Bessel beam. b) same as a) only 50 W ICP for 150 min. c) Etch mixture with CHF_3 : 2.5 Pa process pressure, 180 W ICP, 0 W Bias, 50/10/10 ccm of $SF_6/o_2/CHF_3$. Thickness of Al_2O_3 mask 28.4 nm; Bessel beam was used for ablation. The inset in (c) shows optical images of etched pattern evolution, which turns into colored posts after 60 min of etch.

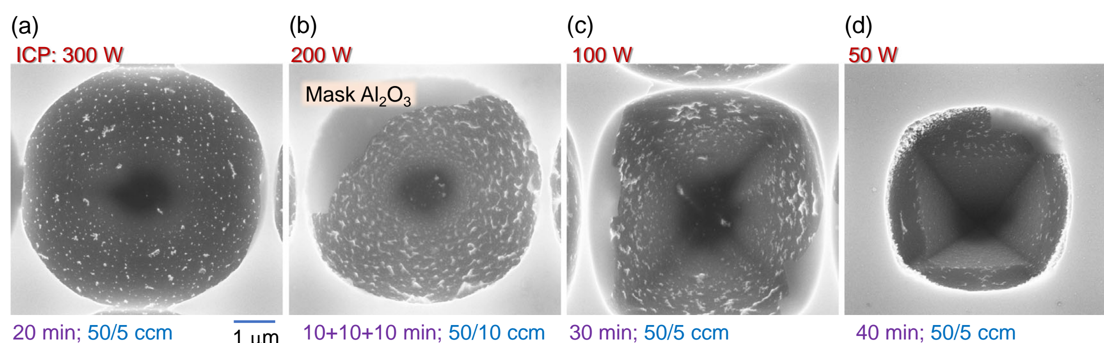

Figure A2. Dependence of etch on ICP power in SF_6/O_2 mixture (ratios are shown at the bottom of panels) at 0 W bias. Representative SEM images of top view after different times of etching. Presence of oxygen shows propensity of oxidation on the etched surface. At low ICP powers, crystallographic structure typical for the Si <001> becomes discernable, see (a) versus (d). The thickness of Al_2O_3 was 38 nm; mask writing by Bessel beam.

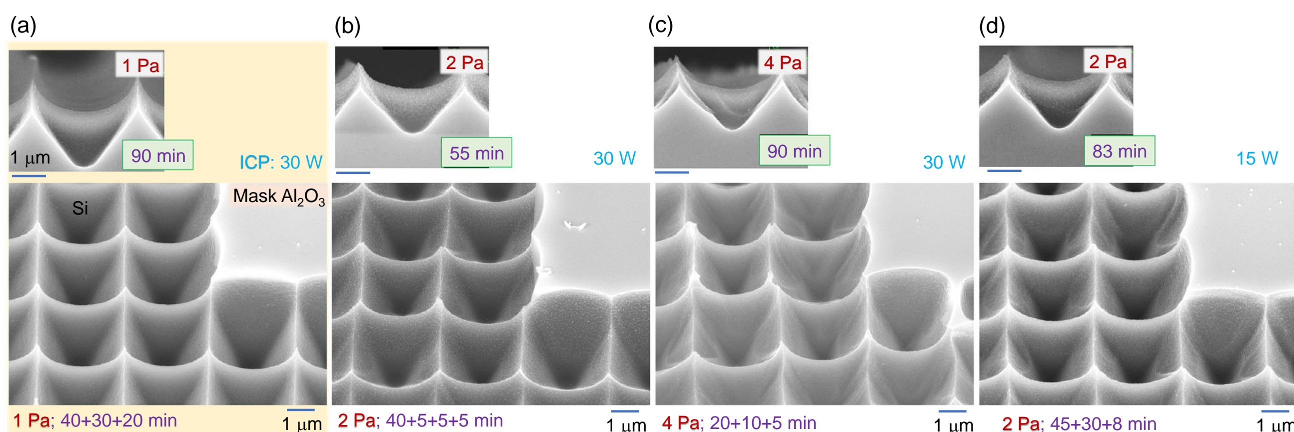

Figure A3. SEM images of etched PhCs on Si at different process pressures: a) 1 Pa, b) 2 Pa, c) 4 Pa, and d) 2 Pa. Top insets show side-view cross section. Etch time is shown at the bottom of panels; when repeated etching was applied, times were shown with a summation marker "+" at the bottom of panels. RIE was carried out at 0 W bias, (a–c) 30 W ICP power and (d) 15 W, at 50/0 ccm SF_6/O_2 gas mixture. Thickness of Al_2O_3 mask was 28.4 nm; mask writing was with Bessel beam. Conditions in (a) were selected for fabrication of PhC light-trapping patterns on solar cells.

© 2024 The Author(s). Advanced Engineering Materials published by Wiley-VCH GmbH

15272648, 2024, 21, Downloaded from https://onlinelibrary.wiley.com/doi/10.1002/adem.202400711 by Vilnius University, Wiley Online Library on [13/11/2024]. See the Terms and Conditions (https://onlinelibrary.wiley.com/terms-and-conditions) on Wiley Online Library for rules of use; OA articles are governed by the applicable Creative Commons License

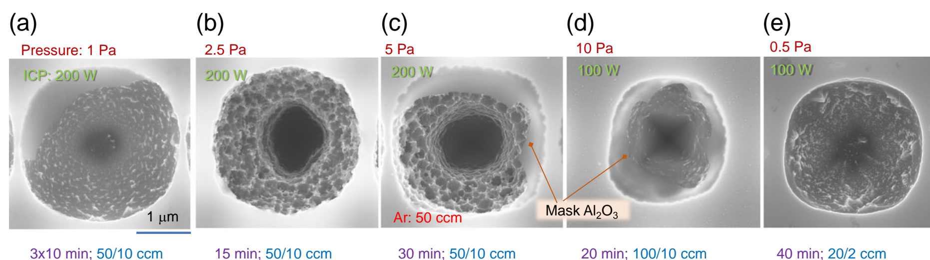

Figure A4. SEM images of etched PhCs on Si at different process pressures: a)1 Pa, b) 2.5 Pa, c) 5 Pa, d) 10 Pa, and e) 0.5 Pa. Etch time is shown at the bottom of panels. RIE was carried out at 0 W bias in all cases, while ICP was 200 and 100 W (marked); Ar at 50 ccm was added for (c). The ratio of flow rate of SF_6/O_2 gas mixture is shown below the panels. Thickness of Al_2O_3 mask was 28.4 nm; mask writing was with Bessel beam.

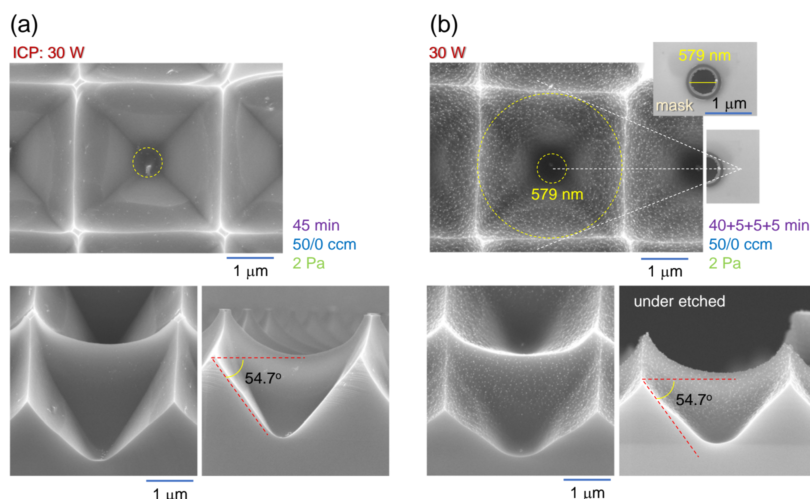

Figure A5. Time, the ratio of flow rate of SF_6/O_2 gas mixture, and pressure are shown. Bias power was 0 W and that of ICP 30 W. a) Single run of etching and b) with three repeated inspections to achieve minimal mesa regions and under etching. Top inset in (b) shows the typical opening in the mask used for this etching with its projections on the etched inverted pyramids as central circles. Thickness of Al_2O_3 mask was 38 nm; mask writing was with Bessel beam. The angle of 54.7° between top surface (100) plane and (111) plane is shown. Repeated exposure to room conditions caused a larger amount of the oxidized residue shown in (b). Under-etching conditions in (b) affected the depth and slope of side walls and was stronger at larger ambient pressure (see Figure A3).

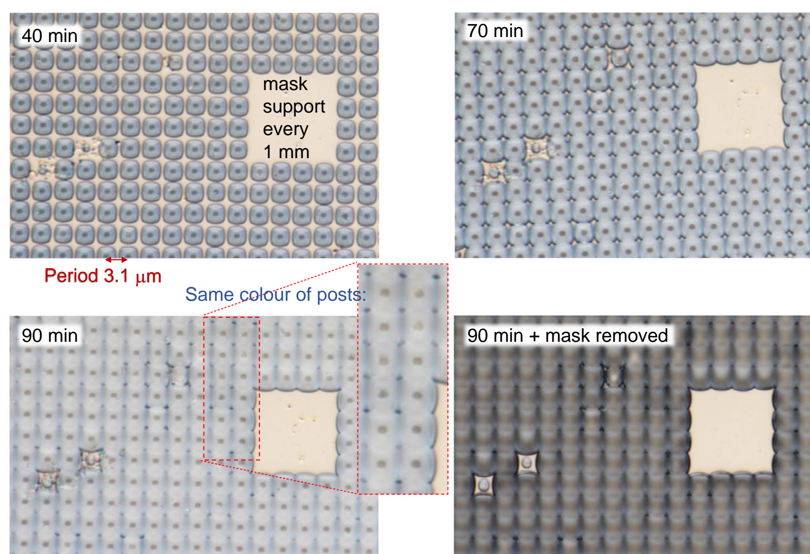

Figure A6. The optimal-etch conditions. Optical images of etching progression for a pressure of 1 Pa, 30 W ICP, 0 W bias, and 50/0 ccm of SF_6/O_2 at the same position on the sample. The smallest corner posts are of the same color (dark blue) observed after 90 min etch; see different colors at conditions of faster etch in Figure 2d. At this condition, etching is stopped and the mask is removed in ultrasonic bath. Thickness of Al_2O_3 mask was 38 nm; mask writing was with Bessel beam.

© 2024 The Author(s). Advanced Engineering Materials published by Wiley-VCH GmbH

15272648, 2024, 21, Downloaded from https://onlinelibrary.wiley.com/doi/10.1002/adem.202400711 by Vilnius University, Wiley Online Library on [13/11/2024]. See the Terms and Conditions (https://onlinelibrary.wiley.com/terms-and-conditions) on Wiley Online Library for rules of use; OA articles are governed by the applicable Creative Commons License

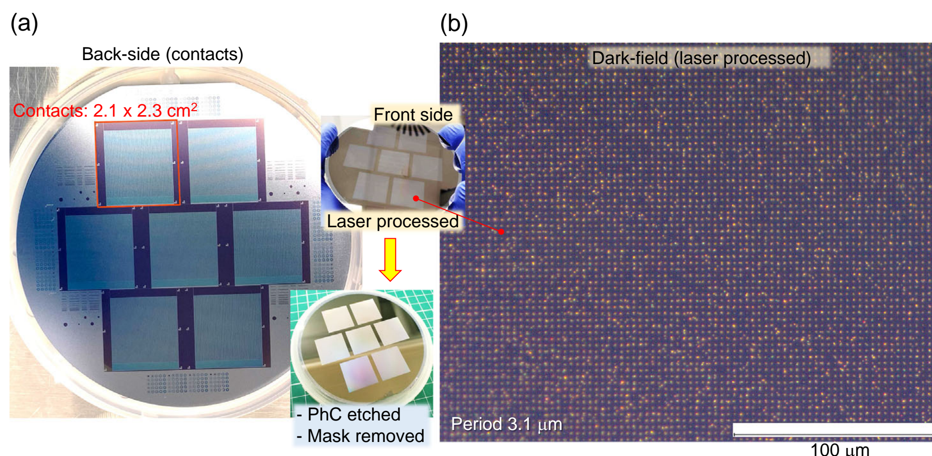

Figure A7. a) Backside view of polysilicon on oxide-interdigitated back-contacted– $POLO^2$–IBC cell with the top-inset image of patterned etch mask by Bessel beam 515 nm/167 fs, pulse energy $E_p = 43.8$ nJ. The thickness of Si solar cell 190 μm. Insets show laser patterned mask and final PhC light-trapping surface and optimized plasma etch and mask removal. b) Optical dark-field image of laser inscribed mask in 38 nm thick Al_2O_3.

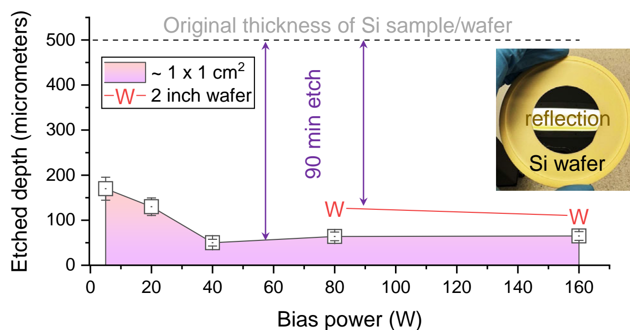

Figure A8. Thinning of 500 μm wafers down to sub-100 μm thickness (Samco ICP-RIE). Plasma thinning of p-type Si at different bias powers, when ICP power was 700 W, process pressure 1 Pa, He back pressure 2 kPa, and etching chemistry SF_6. Etching time was 90 min; error bars 15%. There was a strong dependence on the size of Si substrate, i.e., a centimeter-sized sample was etched 50% faster than a wafer. The cleanest debris-free surface was obtained at the highest bias power of 160 W, when the etch rate was 4.6 μm min^{-1} and the roughness was 25 nm. Noteworthy, n-type Si had a strongly light-scattering appearance at the visible spectral range after etching; the intrinsic and p-type Si was etched identically.

Acknowledgements

The authors would like to acknowledge the support via ARC DP190103284 "Photonic crystals: the key to breaking the silicon-solar cell efficiency barrier" project (S.Ju., S.H.N., S.Jo.). This work was performed in part at the Melbourne Centre for Nanofabrication (MCN) in the Victorian Node of the Australian National Fabrication Facility (ANFF). Support by the German Federal Ministry for Economic Affairs and Climate Protection, research project "27Plus6" (FKZ03EE1056A), is acknowledged.

Open access publishing facilitated by Swinburne University of Technology, as part of the Wiley - Swinburne University of Technology agreement via the Council of Australian University Librarians.

Conflict of Interest

The authors declare no conflict of interest.

Data Availability Statement

The data that support the findings of this study are available from the corresponding author upon reasonable request.

Keywords

Bessel beams, high-efficiency solar-to-electrical energy conversions, Lambertian limits, Si solar cells

Received: March 21, 2024
Revised: July 11, 2024
Published online: August 29, 2024

[1] University of Michigan, Photovoltaic Energy Factsheet, pub. no. css07-08 2023, https://css.umich.edu/publications/factsheets/energy/photovoltaic-energy-factsheet (accessed: March 2024).
[2] T. Saga, *NPG Asia Mater.* **2010**, *2*, 96.
[3] C. Battaglia, A. Cuevas, S. De Wolf, *Energy Environ. Sci.* **2016**, *9*, 1552.
[4] M. Ram, M. Child, A. Aghahosseini, D. Bogdanov, A. Lohrmann, C. Breyer, *J. Cleaner Prod.* **2018**, *199*, 687.
[5] H. Lin, M. Yang, X. Ru, G. Wang, S. Yin, F. Peng, C. Hong, M. Qu, J. Lu, L. Fang, C. Han, P. Procel, O. Isabella, P. Gao, Z. Li, X. Xu, *Nat. Energy* **2023**, *8*, 789.
[6] National Renewable Energy Laboratory (NREL), *Best Research-Cell Efficiency Chart*, https://www.nrel.gov/pv/cell-efficiency.html (accessed: March 2024).
[7] K. Yoshikawa, H. Kawasaki, W. Yoshida, T. Irie, K. Konishi, K. Nakano, T. Uto, D. Adachi, M. Kanematsu, H. Uzu, K. Yamamoto, *Nat. Energy* **2017**, *2*, 17032.
[8] L. Andreani, A. Bozzola, P. Kowalczewski, M. Liscidini, L. Redorici, *Adv. Phys.: X* **2019**, *4*, 1548305.
[9] A. Chutinan, S. John, *Phys. Rev. A* **2008**, *78*, 023825.
[10] P. Kuang, S. Eyderman, M.-L. Hsieh, A. Post, S. John, S.-Y. Lin, *ACS Nano* **2016**, *10*, 6116.
[11] K. Aydin, V. Ferry, R. Briggs, *Nat. Commun.* **2011**, *2*, 517.
[12] M.-L. Hsieh, A. Kaiser, S. Bhattacharya, S. John, S.-Y. Lin, *Sci. Rep.* **2020**, *10*, 11857.

© 2024 The Author(s). Advanced Engineering Materials published by Wiley-VCH GmbH

15272648, 2024, 21, Downloaded from https://onlinelibrary.wiley.com/doi/10.1002/adem.202400711 by Vilnius University, Wiley Online Library on [13/11/2024]. See the Terms and Conditions (https://onlinelibrary.wiley.com/terms-and-conditions) on Wiley Online Library for rules of use; OA articles are governed by the applicable Creative Commons License

[13] J. Maksimovic, J. Hu, S. Ng, T. Katkus, G. Seniutinas, T. Pinedo Rivera, M. Stuiber, Y. Nishijima, S. John, S. Juodkazis, *Opto-Electron. Adv.* **2022**, *5*, 210086.
[14] J. Schäfer, J. Krügener, H. Genath, M. Rosebrock, M. A. Schubert, B. Min, C. Hollemann, R. Peibst, in *14th Int. Conf. on Crystalline Silicon Photovoltaics (SiliconPV)*, Chambery, France, April **2024**.
[15] K. Yamamoto, *JSAP Int.* **2003**, *7*, 12.
[16] M. Bernardi, M. Palummo, J. C. Grossman, *Nano Lett.* **2013**, *13*, 3664.
[17] S. Bhattacharya, S. John, *Phys. Rev. Appl.* **2018**, *9*, 044009.
[18] Y. Li, X. Ru, M. Yang, Y. Zheng, S. Yin, C. Hong, F. Peng, M. Qu, C. Xue, J. Lu, L. Fang, C. Su, D. Chen, J. Xu, C. Yan, Z. Li, X. Xu, Z. Shao, *Nature* **2024**, *626*, 105.
[19] B. Yang, M. Lee, *Opt. Laser Technol.* **2014**, *63*, 120.
[20] J. Maksimovic, H. Mu, D. Smith, T. Katkus, M. Vaičiulis, R. Aleksiejūnas, G. Seniutinas, S. H. Ng, S. Juodkazis, *Micromachines* **2023**, *14*, 550.
[21] S. Eyderman, S. John, A. Deinega, *J. Appl. Phys.* **2013**, *113*, 154315.
[22] A. Deinega, S. Eyderman, S. John, *J. Appl. Phys.* **2013**, *113*, 224501.
[23] P. Mahtani, *Ph.D. Thesis,* School University of Toronto, **2014**.
[24] D. McGloin, K. Dholakia, *Contemp. Phys.* **2005**, *46*, 15.
[25] F. Haase, C. Hollemann, S. Schäfer, A. Merkle, M. Rienäcker, J. Krügener, R. Brendel, R. Peibst, *Sol. Energy Mater. Sol. Cells* **2018**, *186*, 184.
[26] J. Bonse, S. Baudach, J. Krüger, W. Kautek, M. Lenzner, *Appl. Phys. A* **2002**, *74*, 19.
[27] K. Kumar, K. K. C. Lee, P. R. Herman, J. Nogami, N. P. Kherani, *Appl. Phys. Lett.* **2012**, *101*, 222106.
[28] A. Mavrokefalos, S. E. Han, S. Yerci, M. S. Branham, G. Chen, *Nano Lett.* **2012**, *12*, 2792.
[29] L. Jonušauskas, D. Gailevičius, S. Rekštytė, T. Baldacchini, S. Juodkazis, M. Malinauskas,, *Opt. Express* **2019**, *27*, 15205.
[30] B. Voisiat, S. Indrišiūnas, R. Suzanovičienė, I. Šimkienė, G. Račiukaitis, in *Laser Processing and Fabrication for Solar, Displays, and Optoelectronic Devices III*, Vol. *9180* (Ed: E. W. Reutzel), SPIE **2014**, p. 918009.
[31] Q. Wang, P. Yao, Y. Li, L. Jiang, J. Xu, S. Liang, D. Chu, W. He, C. Huang, H. Zhu, H. Liu, *Opt. Laser Technol.* **2023**, *157*, 108647.
[32] S. J. Fonash, *J. Electrochem. Soc.* **1990**, *137*, 3885.
[33] G. Oehrlein, *Mater. Sci. Eng.: B* **1989**, *4*, 441.
[34] G. Kumaravelua, M. M. Alkaisia, D. W. Macdonaldb, J. Zhaoc, B. Rongd, A. Bittare, *Fuel Energy Abstracts* **2006**, *47*, 128.
[35] M. Kim, K. H. Min, S. Park, H. Song, J. I. Lee, K. T. Jeong, J. Park, M. Kang, *Curr. Appl. Phys.* **2020**, *20*, 519.

© 2024 The Author(s). Advanced Engineering Materials published by Wiley-VCH GmbH

15272648, 2024, 21, Downloaded from https://onlinelibrary.wiley.com/doi/10.1002/adem.202400711 by Vilnius University, Wiley Online Library on [13/11/2024]. See the Terms and Conditions (https://onlinelibrary.wiley.com/terms-and-conditions) on Wiley Online Library for rules of use; OA articles are governed by the applicable Creative Commons License